

Nonlinear Contact Control for Space Station Dexterous Arms

Homayoun Seraji, Robert Steele

Jet Propulsion Laboratory
California Institute of Technology
Pasadena, CA 91109, USA

Abstract

In October 1996, a research and development task was initiated at JPL to develop and demonstrate nonlinear contact control schemes for the dexterous robotic arms planned for the Space Station. This paper reports on the progress made to-date in this task. Specifically, the paper introduces a new class of contact controllers comprised of a nonlinear gain in cascade with a linear fixed-gain PI force controller and PD compliance controller. The nonlinear gains used are simple hyperbolic functions of force error and contact force, respectively. The stability of the closed-loop systems incorporating nonlinear PI and PD controllers are investigated using the Popov Stability Criterion. Experimental results are presented to demonstrate the efficacy of the nonlinear force and compliance control schemes for a dexterous 7-DOF Robotics Research arm. These results highlight the advantages of the proposed nonlinear contact controllers compared to linear controllers.

1 Introduction

Over the next few years, the United States, Canada, Russia, Japan, and several European countries will be jointly involved in the assembly of the international Space Station (ISS) in space. This will be the largest collaborative international project in human history. The Space Station will provide a unique vantage point to study the structure and composition of the universe, as well as a microgravity science laboratory in space. During the life of the Space Station, numerous routine maintenance and servicing operations need to be performed on a repetitive and regular basis. These operations include, but are not limited to: inspecting, identifying, grasping, manipulating, relocating and reinserting Orbital Replacement Units (ORU 's) on the Space Station structures, as well as transferring various items

to and from airlocks. The number of Extra Vehicular Activity (EVA) hours that will be spent by astronauts on such routine maintenance operations on the Space Station will directly reduce the crew time available to perform science experiments in space, which is a primary goal for the Space Station.

The key role of the robotic systems planned for the Space Station is to provide the functionality needed to automate the maintenance and servicing operations and thus reduce the crew EVA time spent on such routine activities. The capability of the ISS robotic systems to perform these operations hinges critically on the development and implementation of robust and reliable robotic contact control systems. In fact, robust contact control has been explicitly identified by the ISS Program Office [1] as both a major area of concern and one of the most critical factors in enhancing ISS functionality.

In October 1996, JPL initiated an R&D task that is responsive to this need and specifically aims at the development and demonstration of robust nonlinear contact control schemes that have a high potential to automate the ISS maintenance operations, thereby reducing the crew EVA time. Research on nonlinear contact control is in its infancy at present and only a few papers have been published on the subject [2-4]. The contact control capabilities presented in this paper are targeted for the Special-Purpose Dexterous Manipulator (SPDM) with two 7-DOF arms that will be provided by the Canadian Space Agency for the Space Station [5]. This paper reports on the outcome of the first year of research at JPL. The paper is structured as follows. In Section 2, the position-based contact control system will be described. Nonlinear force and compliance control will be discussed in Sections 3 and 4. Laboratory experimental results are presented in Section 5. Finally, the conclusions drawn from this work are given in Section 6.

2 Position-Based Contact Control Systems

The nomenclature position-based refers to the type of commands given to the manipulator in order to achieve contact control. Position-based strategies can utilize the existing manipulator position control system, retaining safety features and robustness to gravitational, frictional, and inter-joint disturbances [6]. For the Space Station SPDM arms, there is a strong desire to adopt a *non-intrusive* approach for contact control, so that the underlying functional capabilities of the arm position control system are unaffected by the enhancements due to contact control. This approach is also highly desirable from the point of view of ease of implementation, with the contact controller placed in an external feedback loop closed around the internal position control system.

For small free-space motions along a Cartesian axis of interest, the manipulator can be adequately modeled as a positioning device with linear second-order dynamics [6]. The manipulator inertia J_m is due to the effective mass properties of the mechanical system, and the damping and stiffness terms B_m and K_m are primarily due to the F/D-type joint servo controllers in effect around each joint. This leads to the transfer-function model for free-space motion as

$$G(s) = \frac{\Delta x(s)}{\Delta x_c(s)} = \frac{K_s}{J_m s^2 + B_m s + K_m} - \frac{c}{s^2 + as + b} \quad (1)$$

where Δx_c and Δx denote changes in the commanded and the actual positions of the end-effector along the motion axis, $a = B_m/J_m$, and $c = K_m/J_m$. During the end-effector contact with the environment, the end-effector dynamics is modified due to the contact force F measured by the force/torque sensor mounted on the manipulator wrist. The environment is modeled as a pure stiffness K_e , since in many contact tasks the inertia and damping effects are insignificant compared to the level of stiffness. Let K_s denote the stiffness of the force/torque sensor. Then, the measured contact force F obeys the Hooke's law as

$$F = (K_s^{-1} - K_e^{-1})^{-1} \Delta x = K_c \Delta x \quad (2)$$

where Δx represents the end-effector penetration into the environment. Due to the contact force, the end-effector dynamics is modified to

$$J_m \Delta \ddot{x} + B_m \Delta \dot{x} + K_m \Delta x = K_m \Delta x_c - F$$

which leads to the transfer-function model during contact as

$$\hat{G}(s) = \frac{\Delta x(s)}{\Delta x_c(s)} = \frac{c}{s^2 + as + b} \quad (3)$$

where $b = \frac{K_s + K_e}{J_m}$. Observe that the environmental stiffness K_e changes the dynamics of the end-effector position control system at contact, to an extent depending on the relative sizes of K_m , K_s , and K_e . From equations, (2) and (3), the contact force/position command model is given by

$$\hat{G}(s) \cdot \frac{F(s)}{\Delta x_c(s)} = \frac{cK_c}{s^2 + as + b} \quad (4)$$

In this paper, we shall consider two distinct approaches to contact control, namely *force control* and *compliance control*. In force control, the force setpoint F_r is specified by the user and is tracked *explicitly* by the force controller. In compliance control, on the other hand, the reference position Δx_r is used to control the contact force F implicitly. These two approaches are described in the following sections.

3 Nonlinear PI Force Control

Figure 1 depicts the block diagram of the position-based nonlinear force control system proposed in this paper. The force controller consists of the nonlinear gain k preceding the linear fixed-gain proportional-integral (PI) controller $K(s) = k_p + k_i/s$, where k_p and k_i are positive constants and the gain k is a function of the force error $e = F_r - F$. The nonlinear gain k acts on the force error $e(t)$, and produces the "scaled" error $f(t) = k(e)e(t)$. The scaled error $f(t)$ is then inputted to the PI controller $K(s)$ which generates the position perturbation x_f that is used to modify the reference position Δx_r in real time. The gain k can represent any nonlinear function which is bounded in the sector $0 \leq k \leq k_{max}$. There is a broad range of options available for the nonlinear gain k . In this paper, we propose the gain k to be the *hyperbolic* function of the error e as

$$k = k_0 - \frac{2k_1}{\exp(k_2 e) + \exp(-k_2 e)} = k_0 - k_1 \operatorname{sech}(k_2 e) \quad (5)$$

where k_0 , k_1 , and k_2 are user-defined positive constants. The gain k is upper-bounded by k_0 , which is reached to within 1% when $|e| \geq 5/k_2$, and is lower-bounded by $k_0 - k_1$ when $e = 0$. Thus k_0 defines the *maximum value*, k_1 denotes the *range of variation*, and k_2 specifies the *rate of variation* of k . Figure 2 shows a typical variation of k versus e when $k_0 = 4$, $k_1 = 3$, and $k_2 = 0.05$. It is seen that k is an "inverted bell-shaped" curve, and is an even

function of e , that is $k(-e) = k(e)$, which implies that k is a function of the error magnitude $|e|$.

Consider now the closed-loop force control system shown in Figure 1. Because of the nonlinear nature of k , the stability analysis of the closed-loop system is non-trivial. To investigate the absolute stability of the closed-loop system, we combine the linear components $G(s)$ and $K(s)$ as

$$W(s) = \bar{G}(s)K(s) = \frac{c(k_p s + k_i)}{s(s^2 + as + b)} \quad (6)$$

which is a third-order transfer-function, and separate out the nonlinear element which is the gain k . We can now apply the Popov Stability Criterion [7] to the system by examining the Popov plot of $W(j\omega)$, which is the plot of $\text{Re}W(j\omega)$ versus $\omega \text{Im}W(j\omega)$, with the frequency ω as a parameter and Re and Im refer to the real and imaginary parts, respectively. This plot reveals the range of values that the nonlinear gain k can assume while retaining closed-loop stability. The Popov Criterion can be stated graphically as follows:

“A *sufficient* condition for the closed-loop system to be absolutely stable for all nonlinear gains in the sector $0 \leq k \leq k_{max}$ is that the Popov plot of $W(j\omega)$ lies entirely to the right of a straight-line passing through the point $-\frac{1}{k_{max}} + j0$.”

In order to apply the Popov Criterion to the system, we need to compute the crossing of the Popov plot of $W(j\omega)$ with the real axis. From equation (6), we obtain

$$\text{Re}W(j\omega) = \frac{-c[k_p \omega^2 + (ak_i - bk_p)]}{a^2 \omega^2 + (b - \omega^2)^2} \quad (7)$$

$$\omega \text{Im}W(j\omega) = \frac{-c[(ak_p - k_i)\omega^2 + bk_i]}{a^2 \omega^2 + (b - \omega^2)^2} \quad (8)$$

Two distinct cases are now possible depending on the relative values of k and k_p .

3.1 Case One: $k_i \leq ak_p$

In this case, $\omega \text{Im}W(j\omega)$ is *always* negative for all ω , that is, the Popov plot of $W(j\omega)$ remains entirely in the third and fourth quadrants and does *not* cross the real axis. This implies that we can construct a straight-line passing through the origin such that the Popov plot is entirely to the right of this line. Therefore, according to the Popov Criterion, the range of the allowable nonlinear gain k is $(0, \infty)$.

3.2 Case Two: $k_i > ak_p$

In this case, the Popov plot of $W(j\omega)$ crosses the real axis. The crossover frequency ω_c is obtained by solving

$\omega_c \text{Im}W(j\omega_c) = 0$, and the *maximum* allowable gain is found to be

$$k_{max} = \frac{1}{\text{Re}W(j\omega_c)} = \frac{ab}{(k_i - ak_p)c} \quad (9)$$

Thus the range of the allowable nonlinear gain k is $(0, k_{max})$. Notice that k_{max} given by equation (9) represents a conservative bound on the nonlinear gain, because the Popov criterion gives a sufficient condition for stability. Applying the Popov Criterion to the hyperbolic function (5) yields the following stability conditions:

$$k_1 \leq k_0 \leq k_{max} \quad (10)$$

The nonlinear PI force controller ensures that the contact force F responds to the force setpoint F_r with a small rise time and a low overshoot, and F settles rapidly to F_r with zero steady-state error. The contact force F is also unaffected in the steady-state by step changes in the reference position Δx_r . Furthermore, the steady-state force tracking and position rejection features are maintained despite variations in the system parameters, provided the closed-loop system retains stability. The performance of the nonlinear PI force controller is demonstrated in the experimental studies reported in Section 5.1.

4 Nonlinear PD Compliance Control

The block diagram of the nonlinear compliance control system proposed in this paper is shown in Figure 3. The contact force F measured by the wrist-mounted force/torque sensor is acted upon by the nonlinear gain k to produce the “scaled” force signal $f(t) = k(F) F(t)$, where the gain k is a function of the force F . This signal is then inputted to the linear fixed-gain proportional-derivative (PD) controller $K(s) = k_p + s k_d$, which generates the position perturbation x_f that modifies the reference position Δx_r in real time, where k_p and k_d are positive constants. In practice, the measured contact force is initially passed through a first-order low-pass filter to remove the measurement noise prior to differentiation. The gain k can represent any nonlinear function which is bounded in the sector $0 \leq k \leq k_{max}$. There is a broad range of options available for the nonlinear gain k . As in Section 3, we choose the gain k to be the *hyperbolic* function of the contact force F as

$$k = k_0 - \frac{2k_i}{\exp(k_2 F) + \exp(-k_2 F)} = k_0 - k_1 \text{sech}(k_2 F) \quad (11)$$

where k , k_p , and k_d are user-defined positive constants. It is seen that k is an even function of F , that is $k(-F) = k(F)$, which implies that k is bi-directional and behaves the same when pushing on the environment ($F > 0$) or pulling off the environment ($F < 0$).

We shall now investigate the absolute stability of the closed-loop system. We combine the linear components $G(s)$ and $K(s)$ as

$$w(s) = \bar{G}(s)K(s) = \frac{c(k_p + k_d s)}{s^2 + as + b} \quad (12)$$

which is a second-order transfer-function, and separate out the nonlinear element which is the gain k . To find out the range of values that "the nonlinear gain k can assume while retaining closed-loop stability, we examine the Popov plot of $W(j\omega)$. From equation (12), we obtain

$$\text{Re}W(j\omega) = \frac{c[(ak_d - k_p)\omega^2 + bk_p]}{a^2\omega^2 + (b - \omega^2)^2} \quad (13)$$

$$\text{Im}W(j\omega) = \frac{-c\omega^2[k_d\omega^2 + (ak_p - bk_d)]}{a^2\omega^2 + (b - \omega^2)^2} \quad (14)$$

Two cases are now possible depending on the relative values of k_p and k_d .

4.1 Case One: $bk_d \leq ak_p$

In this case, from equation (14) it is seen that $\text{Im}W(j\omega)$ is *always* negative for all non-zero ω , that is, the Popov plot of $W(j\omega)$ remains entirely in the third and fourth quadrants and does *not* cross the real axis. Therefore, according to the Popov Criterion, the range of the allowable nonlinear gain k is $(0, \infty)$.

4.2 Case Two: $bk_d > ak_p$

In this case, the Popov plot of $W(j\omega)$ crosses the real axis. The crossover frequency ω_c is obtained by solving $\omega_c \text{Im}W(j\omega_c) = 0$, and the value of $W(j\omega_c)$ is then found to be

$$\text{Re}W(j\omega_c) = \frac{ck_d}{a} \quad (15)$$

which is always positive. Since the Popov plot of $W(j\omega)$ never crosses the *negative* real axis, from the Popov Criterion the range of the allowable nonlinear gain k is $(0, \infty)$.

We conclude that in both cases, the closed-loop system is always stable under nonlinear PD compliance control with unbounded nonlinear gain k . The performance of the nonlinear PD compliance controller is demonstrated in the experimental studies in Section 5.2.

5 Experimental Studies

The nonlinear force and compliance control schemes developed in Sections 3 and 4 are implemented on the Robotics Research Corporation (RRC) arm shown in Figure 4. This section describes the laboratory setup and the real-time computing platform used for the force and compliance control studies, as well as the experimental results obtained.

The laboratory setup consists of the RRC model K-1207 7-DOF arm that emulates the SPDM arm, a wrist-mounted force/torque sensor, a VME-based computing platform, and a SUN Ultra1 workstation. There is a one-third scale mock-up of part of the Space Station truss structure in the arm workspace with ORU's, solar panels, and solar blankets that represent typical contact surfaces available on the Space Station. The RRC arm is controlled by the VME-based real-time controller that hosts the Configuration Control algorithm [8] for task-space dexterous motion control. The Configuration Control approach is implemented as the baseline Cartesian position control system for the arm, and ensures that the end-effector position and orientation and the arm angle track user-defined trajectories accurately. The real-time controller uses two Motorola MC68060 processors along with various data acquisition, shared memory, and communication cards. This controller is linked via socket communication to the SUN Ultra1 workstation, which serves as the host computer for the user interface. The controller is also interfaced directly with the Multibus-based RRC arm control unit via a high-speed bus interface. The real-time controller computes the seven joint setpoints every 1.1msec; however, the RRC Servo Level Interface is set up to run at the sampling frequency of 400Hz, i.e., the joint setpoints are updated every 2.5msec.

A model 15/50 Assurance Technologies Inc. (ATI) 6-axis force/torque sensor is mounted on the wrist of the RRC arm. During contact with a reaction surface, this sensor continuously measures the end-effector contact forces and torques, and deposits this information in the shared memory card of the arm control system. The first-order low-pass filter $\frac{1}{0.05s+1}$ is used in the control software to remove the high-frequency noise superimposed on the force measurement. At each sampling instant, the contact control software acquires the current contact force F (and the user-specified force setpoint F_r , if appropriate) and generates the position perturbation x_f based on the contact control algorithms developed in Sections 3 and 4. The detailed description of the control software is given in [9]. We shall now describe the force and compliance control experiments separately.

5.1 Force Control Experiments

In the force control experiments, the end-effector is commanded to: move down under explicit force control, make contact with a steel plate resting on a table that emulates the ORU surface stiffness, apply a force setpoint of $F_r = 10Nt$ initially followed by $F_r = 40Nt$, and then retract from the surface. The PI force control law used is

$$x_f(t) = 10^{-3} \left\{ k_p [k(e)e(t)] + k_i \int_0^t [k(e) e(t)] dt \right\} \quad (16)$$

where $e = F_r - F$ is the force error, $k_p = 0.05$, $k_i = 0.5$, and 10^{-3} converts the controller output from millimeter to meter. The response of the contact force F using the fixed-gain PI controller with $k(e) = 4$ is shown in Figure 5a. It is seen that the contact force rises rapidly to $40Nt$, but has some oscillations about the setpoint with the peak overshoot of $M_p = 30\%$, and the response settles to the steady-state value of $40Nt$ in $t_s = 1.10$ sccs.

To demonstrate the effect of the nonlinear gain $k(e)$, the experiment is repeated with k as a hyperbolic function of e , that is

$$k = 4 - \frac{6}{\exp(0.05e) + \exp(-0.05e)} \quad (17)$$

where k can now vary in the range $1 \leq k \leq 4$, and k versus e is plotted in Figure 2. Figure 5h shows the variation of the nonlinear gain k as a function of time during the experiment. It is seen that the gain k starts at the initial value of 2.25 when $e = 30$. However, as the time proceeds and the error is reduced, the nonlinear gain is automatically decreased and ultimately settles to the final value of 1.0 when $e = 0$. The step response of the contact force using the nonlinear gain (17) is shown in Figure 5c. It is evident that the contact force responds rapidly, but due to the automatic reduction of k , the peak overshoot is now reduced to $M_p = 1\%$ and the response settles quickly to the steady-state value of $40Nt$ in $t_s = 0.92$ secs without any oscillations.

In comparing the performances of the fixed-gain and the nonlinear-gain PI controllers used in these experiments, we conclude that the peak overshoot and oscillations of the force response are significantly decreased *without compromising the speed of the force response*. This is due to the automatic adjustment of the gain k , which prevents oscillations in the force response by reducing the gain as the force response approaches the setpoint. This gain reduction is primarily responsible for the decrease in the overshoot and the oscillations. Observe that the nonlinear PI controller enjoys the advantage of a high initial k to obtain a fast response, but

does not suffer from the disadvantage of excessive oscillations. With a large overshoot which often accompanies a fast response when fixed-gain controllers are used.

5.2 Compliance Control Experiments

In the compliance control experiments, the end-effector is commanded to: move down under compliance control, make initial contact with a reaction surface resting on a table, apply the reference position of $\Delta x_r = 30mm$, and then retract from the surface. Two types of reaction surfaces are considered: a soft foam and a steel plate. These two surfaces emulate, respectively, the stiffnesses of the solar blanket and the ORU surface on the Space Station. The PD compliance control law used is

$$x_f(t) = 10^{-3} \left\{ k_d \frac{d}{dt} [k(F)F(t)] + k_p [k(F)F(t)] \right\} \quad (18)$$

where $k_d = 0.01$ and $k_p = 0.5$. Using the fixed-gain PD controller with $k(F) = 1$, for $\Delta x_r = 30mm$ the apparent stiffness $k_{ap} = \frac{\Delta F}{\Delta x_r}$ of the foam and steel surfaces are found to be

$$k_{foam} = 1.15Nt/mm ; \quad k_{steel} = 1.76Nt/mm \quad (19)$$

It is seen that the apparent stiffness of the contact surface as seen by the reference position Δx_r changes significantly from 1.15 to 1.76 when a fixed-gain compliance controller is used.

The experiment is now repeated with the nonlinear gain k as a hyperbolic function of F , that is

$$k = 3 - \frac{4}{\exp(0.05F) + \exp(-0.05F)} \quad (20)$$

This allows the nonlinear gain k to vary in the range $1 \leq k \leq 3$ depending on the contact force F . Using the nonlinear PD controller, the apparent surface stiffnesses are now found to be

$$k_{foam} = 0.62Nt/mm ; \quad k_{steel} = 0.79Nt/mm \quad (21)$$

In comparison with the fixed-gain case, it is evident that due to the automatic adjustment of the gain k , the nonlinear PD controller has reduced the sensitivity of the apparent stiffness to the change in the surface stiffness. The variation of the nonlinear gain k during contact with the steel plate is depicted in Figure 6. The nonlinear characteristic of k is directly responsible for the reduction in sensitivity of the apparent stiffness when contacting different surfaces.

6 Conclusions

Position-based contact control is a pragmatic and convenient method of providing controlled contact using an existing position or rate-controlled manipulator. The Cartesian control is augmented by an outer feedback loop that senses contact forces and alters the Cartesian commands according to the contact task specifications.

The attractive feature of the nonlinear force controller proposed in this paper is the ability to produce a fast force response with a low overshoot and a small settling time. This is due to the nonlinear characteristic of the gain used in the control scheme. The nonlinear compliance controller introduced here has the advantage of reducing the sensitivity of the apparent stiffness to gross changes in the surface stiffness. The features of the proposed controllers are demonstrated in the experimental studies reported in the paper.

Current research at JPL is aimed at further development and evaluation of the nonlinear force and compliance control schemes for execution of typical Space Station contact tasks. The outcome of this work will be transferred to the NASA-Johnson Space Center and the Canadian Space Agency for implementation on the SPDM arm control system.

7 Acknowledgment

The research described in this paper was carried out at the Jet Propulsion Laboratory, California Institute of Technology, under contract with the National Aeronautics and Space Administration.

8 References

1. J. Temple: "Space Station requirements for advanced engineering and technology development", ISS Program Office, Dec. # SSP-50198, NASA-JSC, 1995.
2. H.P. Qian and J. De Schutter: "Introducing active linear and nonlinear damping to enable stable high gain force control in case of stiff contact", Proc. IEEE Intern. Conf. on Robotics and Automation, vol. 2, pp. 1374-1379, Nice (France), 1992.
3. Y. Xu, D. Ma, and J.M. Hollerbach: "Nonlinear proportional and derivative control for high disturbance rejection and high gain force control", Proc. IEEE Conf. on Robotics and Automation, vol. 1, pp. 752-759, Atlanta, 1993.
4. L.S. Wilfinger, J.T. Wen, and S. Murphy: "Integral force control with robustness enhancement", Proc. IEEE Intern. Conf. on Robotics and Automation, vol. 1, pp. 100-105, Atlanta, 1993.
5. M.E. Stieber, C. F. Trudel, and D.G. Hunter: "Robotic systems for the International Space Station", Proc. IEEE Intern. Conf. on Robotics and Automation, vol. 4, pp. 3068-3073, Albuquerque, 1997.
6. A. Lawrence and R.M. Stoughton: "Position-based impedance control: Achieving stability in practice", Proc. AIAA Guidance, Navigation, and Control Conf., pp. 221-226, Monterey, 1987.
7. K.S. Narendra and J.H. Taylor: *Frequency Domain Criteria for Absolute Stability*, Academic Press Publishers, New York, 1973.
8. H. Seraji, M. Long, and T. Lee: "Motion control of 7-DOF arms: The configuration control approach", IEEE Trans. on Robotics and Automation, vol. 9, no. 2, pp. 125-139, 1993.
9. H. Seraji, D. Lim, and R. Steele: "Experiments in contact control", Journal of Robotic Systems, vol. 13, no. 2, pp. 53-73, 1996.

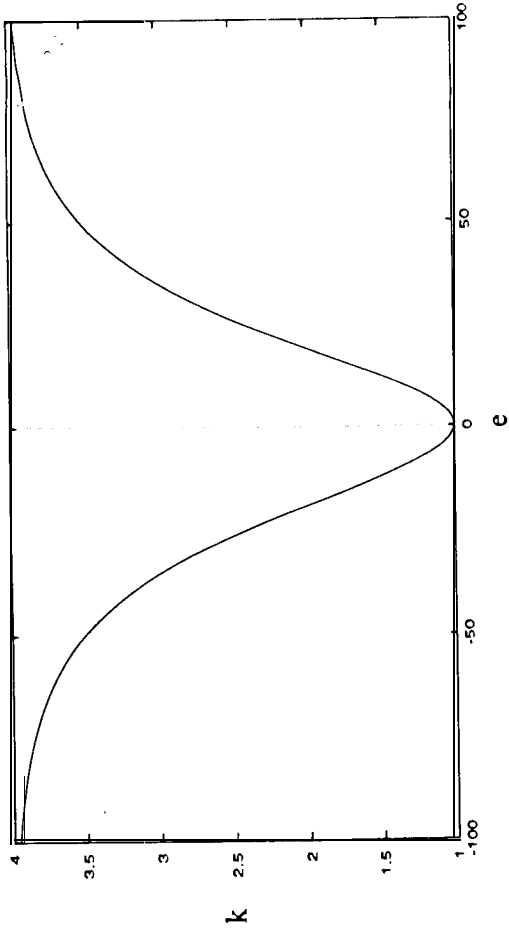


Figure 2. Variation of k versus e

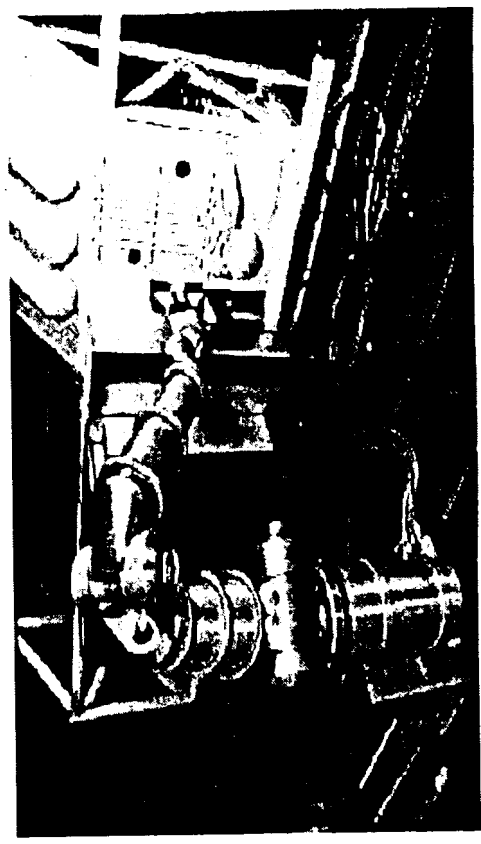


Figure 4. Laboratory Setup for Contact Control Experiments

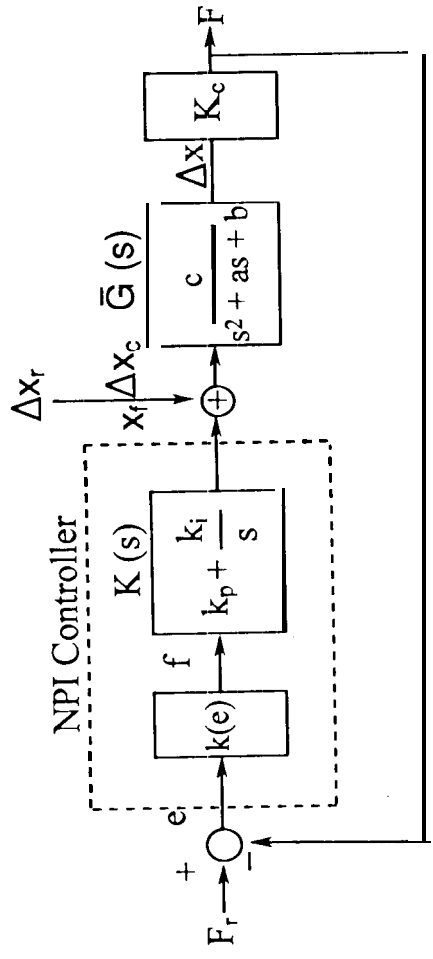


Figure Nonlinear Force Control System

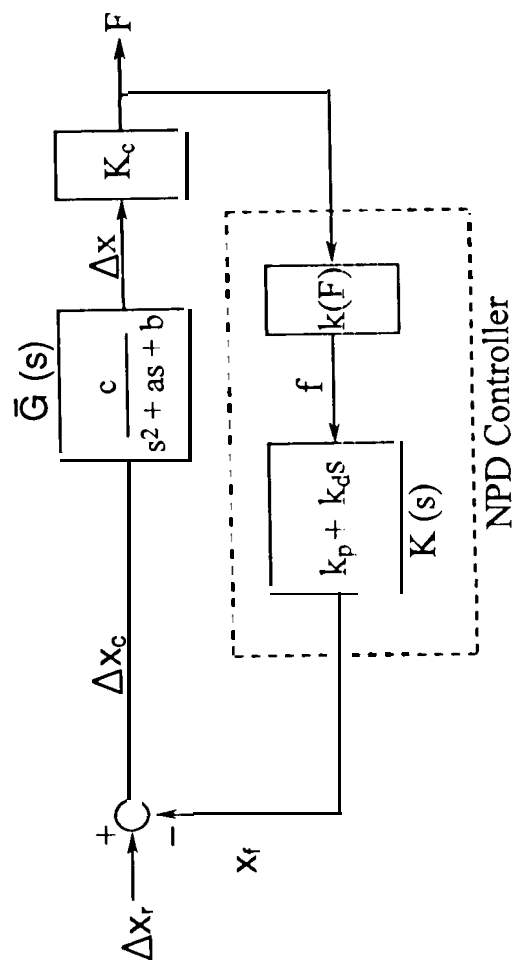


Figure 3 - Nonlinear Compliance Control System

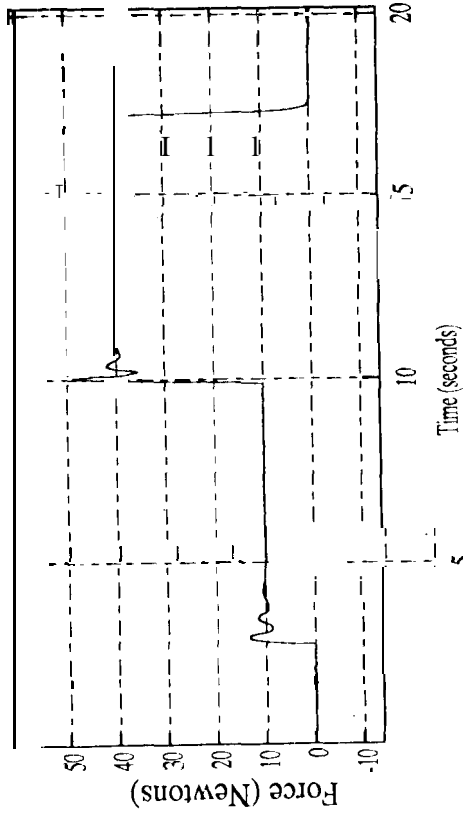


Figure 5a. Force Response using a Fixed-Gain PI Controller

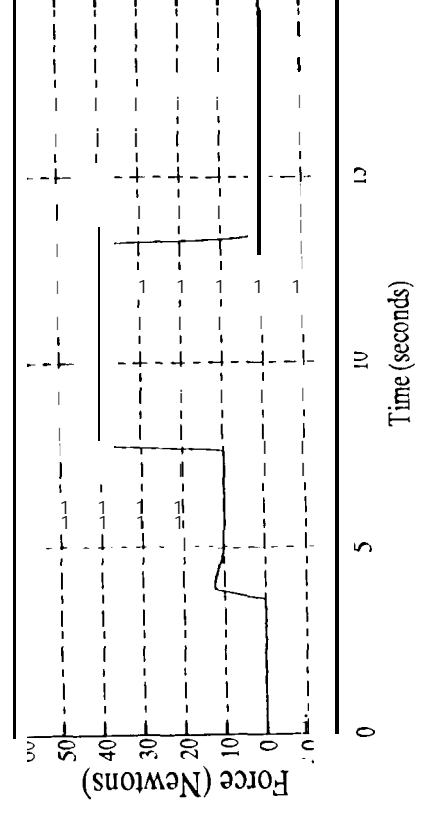


Figure 5c. Force Response using a Non-linear PI Controller

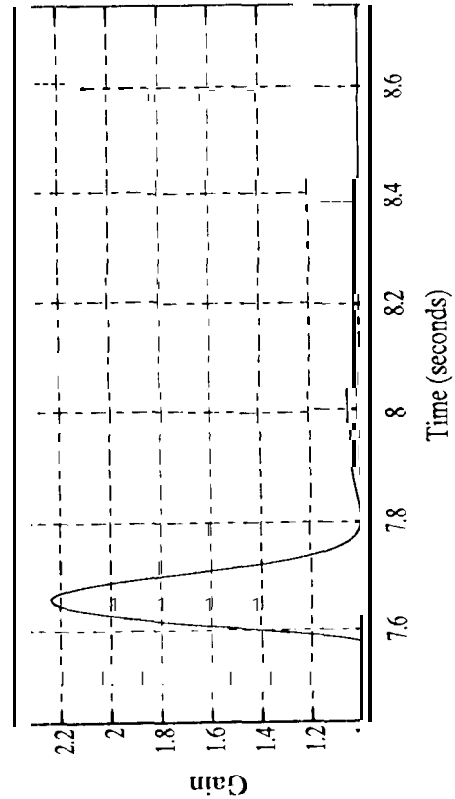


Figure 5b. Variation of Gain in Force Control

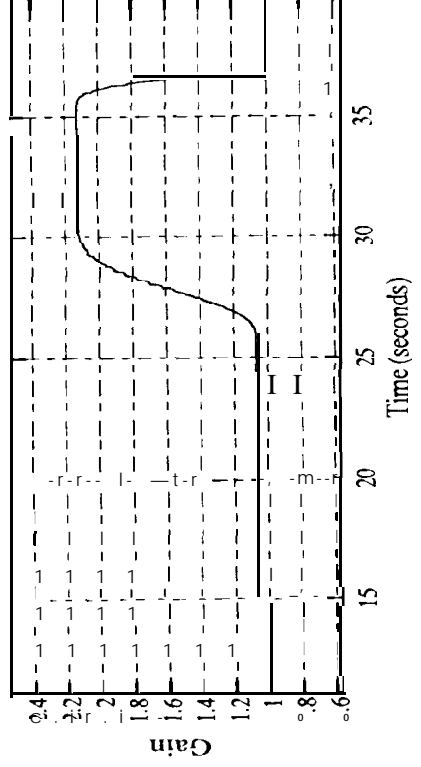


Figure 6. Variation of Gain in Compliance Control